Am J Transl Res 2024;16(9):4589-4600
www.ajtr.org /ISSN:1943-8141/AJTR0158283

Original Article

Multimodal ultrasound imaging of a rat model with ischemic heart failure and its relationship to histopathology

Qiufang Ouyang[1], Rong Xu[1], Qing Lin[1], Jinxian Yan[2], Luting Zhang[1], Hongjia Zhao[3]

[1]Ultrasound Department, The Second Affiliated Hospital of Fujian University of Traditional Chinese Medicine, Fuzhou 350003, Fujian, China; [2]Key Laboratory of Chinese Medicine Preparation for Medical Institutions in Fujian Province (Fujian University of Traditional Chinese Medicine), Fuzhou 350003, Fujian, China; [3]Fujian University of Traditional Chinese Medicine, Fuzhou 350122, Fujian, China

Received June 5, 2024; Accepted August 30, 2024; Epub September 15, 2024; Published September 30, 2024

Abstract: Objective: To investigate the value of multimodal ultrasound imaging in assessing ischemic heart failure, and to analyze the relationship between ultrasound parameters and histopathology. Methods: Thirty male healthy SD rats were randomly divided into a control (n = 10) and a model group (n = 20). The rat model of ischemic heart failure (IHF) was established by the ligation of left anterior descending artery for 4 weeks. Left ventricular ejection fraction (LVEF) and left ventricular cardiac output (LVCO) were determined with routine echocardiography. Global longitudinal strain (GLS) and global circumferential strain (GCS) were determined with Speckle Tracking. Myocardial oxygen saturation (sO_2) was measured with photoacoustic (PA) imaging. Hematoxylin and eosin (H&E) staining, transmission electron microscopy, and Masson staining were performed to determine mitochondrial damage and myocardial fibrosis. Enzyme-linked immunosorbent assay (ELISA) was performed to detect the serum levels of cardiac troponin I (cTNT) and N-terminal B-type natriuretic peptide (NT-pro BNP). Pearson correlation analysis was employed to analyze the correlation among LVEF, LVCO, GLS, GCS, sO_2, mitochondrial impairment, fibrosis, cTNT and NT-pro BNP. Results: Echocardiography revealed significant systolic function changes in the model group as compared to the control group, characterized by decreased LVEF and CO. The serum levels of cTn-T and NT-proBNP were increased, suggesting myocardial injury and functional impairment. GLS and GCS in the model group was reduced as compared to the control group. Concurrently, a marked reduction in sO_2 was observed in the anterior wall of the model rats, whereas that in the posterior wall showed no significant change. Histopathologic examinations unveiled pronounced cellular and subcellular damage, such as disorganization of myocardial fibers and mitochondrial impairment, with the model group presenting a higher Flameng score. Masson's trichrome staining revealed increased myocardial fibrosis. Correlation analyses pinpointed significant associations between echocardiographic parameters, degree of mitochondrial damage, fibrosis, and the levels of cTn-T and NT-proBNP in the model group. This indicated the interrelated nature of structural changes and functional impairment in IHF. Notably, GLS showed the strongest correlations with indicators of myocardial injury. However, anterior wall sO_2 did not demonstrate a significant correlation with either histopathologic damage or serum biomarker levels. Conclusions: Myocardial GLS is a sensitive indicator of pathological myocardial remodeling in heart failure. The multimodal ultrasound can be applied to assess pathologic remodeling in IHF rats.

Keywords: Echocardiography, ischemic heart failure, fibrosis, rats, strain, oxygen saturation

Introduction

Ischemic heart failure (IHF), a significant consequence of myocardial infarction, contributes substantially to mortality, with a notable five-year all-cause death rate of 55.40% [1]. IHF is characterized by high morbidity and rehospitalization rate and has become a pressing public health challenge worldwide [2]. Extensive preclinical investigations have been conducted to elucidate the pathophysiologic mechanisms underlying IHF, predominantly employing post-MI animal models induced by the ligation of the left anterior coronary artery [3]. However, the use of this model is constrained by its limited controllability, resulting in high mortality rates

https://doi.org/10.62347/FIWE8677

and variability in cardiac function impairment [4]. Therefore, accurate evaluation of cardiac function in IHF models is essential for experimental reproducibility and stability.

Ultrasonography, which is radiation-free, cost-effective, and portable, is extensively used in the diagnosis and management of cardiac diseases [5]. Routine ultrasound effectively assesses cardiac structures and functions but has relatively low sensitivity to subtle alterations in cardiac function. To overcome this limitation, strain imaging has emerged as a valuable tool for quantitatively analyzing myocardial motion [6]. By automatically tracking the positions of myocardial tissues along the ventricular wall and computing myocardial deformation, strain imaging provides an objective and accurate reflection of myocardial movement. Myocardial global longitudinal strain (GLS) has been identified as an early indicator of cardiac interstitial fibrosis in hypertensive rodent models. Fu et al. demonstrated a correlation between GLS and collagen volume fraction (CVF) in spontaneously hypertensive rats, highlighting the potential of GLS to assess myocardial fibrosis [7]. Additionally, photoacoustic (PA) ultrasound offers a novel approach to evaluate local oxygenation status, providing valuable insight into tissue oxygenation levels [8, 9]. Despite the utility of these techniques, there remains a paucity of studies utilizing multimodal ultrasonic approaches, which combine strain imaging and PA ultrasound, for the assessment of IHF models [10]. Furthermore, limited research directly compares myocardial strain parameters and tissue oxygen saturation (sO_2) with mitochondrial damage, fibrosis, cardiac troponin T (cTnT), and pro-B-type natriuretic peptide (pro-BNP) levels in IHF models.

Echocardiography is a first-line imaging examination technique for the diagnosis and monitoring of heart failure. It allows for evaluation of myocardial malformations, thereby assessing global and regional cardiac function. The analysis of myocardial deformation has transitioned from tissue Doppler imaging technology to multimodal ultrasound imaging technology. Despite significant improvements in the treatment options for heart failure, the all-cause mortality rate remains high, with 12-month rates of 17% for hospitalized patients and 7% for stable or non-bedridden patients. Ischemic heart disease is the most common cause of heart failure and has a poorer prognosis compared to non-ischemic heart failure. Given the likely need for specialized treatment strategies for IHF, distinguishing it from non-ischemic heart failure is crucial. Multimodal ultrasound imaging, with the ability to analyze myocardial mechanics, presents a cost- effective imaging method. However, there is a lack of sufficient data on its applicability and clinical relevance in the differential diagnosis of ischemic cardiomyopathy and non-ischemic cardiomyopathy.

In this investigation, we developed an IHF model induced by left anterior descending (LAD) artery ligation. The multimodal ultrasonic approach and histopathologic analysis were employed to evaluate this model. By integrating strain imaging and PA ultrasound techniques, we seek to elucidate the relationship between ultrasound indices and key pathologic markers of IHF progression, thereby offering a precise imaging evaluation methodology for cardiac function.

Materials and methods

Experimental animals

All of the procedures and protocols were approved by *Institutional Animal Care and Use Committee, Fujian University of Traditional Chinese Medicine (FJPSPH-IAEC2019061)*. 8-week-old male Sprague-Dawley rats (Shanghai PooleBikai Laboratory Animal Co., Ltd. License No.SCXK2018-0006), weighing 180-220 g, were used. Animals were kept on a 12/12 h light/dark cycle and received water and food *ad libitum*.

Preparation of IHF rat model

After one week of acclimatization, rats were randomly allocated to either a control group (n = 10) or an IHF group (n = 20). Rats were placed in an induction chamber and anesthetized with 3% isoflurane until the disappearance of the toe pinch reflex. Subsequently, the rats were restrained and maintained under anesthesia with a 3% isoflurane mask.

Following fur removal and skin disinfection, a 2.5 cm transverse incision was made between the third and fourth intercostal spaces on the left side of the sternum. Muscles were dissected to expose the heart apex, and a permanent

ligation was performed on LAD artery 2.0-2.5 mm below the junction between the conus arteriosus and the left atrial appendage using a 6/0 nylon suture with a curved needle [11]. The success of the ligation was confirmed by observing a pale infarct area, weakened ventricular wall motion, and sustained ST-segment elevation with a monophasic pattern in limb leads on a real-time electrocardiogram (ECG). In contrast, the control rats received only a puncture below the LAD without ligation. After removal of the retractors, air was expelled from the thoracic cavity, and the muscle and skin layers were sutured sequentially. Postoperatively, the rats were placed on a heating pad at 37°C for recovery. Four weeks post-ligation, echocardiography was performed to evaluate cardiac function in the rats. Then, left ventricular (LV) tissue and serum samples were collected for pathologic and serological analysis.

Routine echocardiographic assessment of left ventricular function

Transthoracic echocardiography was conducted on rats under 1.5% isoflurane anesthesia with an ultrasound system (Vevo 3100, VisualSonics) as previously reported [12]. The rats were placed on a heating platform to maintain the temperature at 37°C. The mean value of three consecutive cardiac cycles was measured. M-mode images of short-axis sections of papillary muscles were used to measure the following indices: interventricular septal thickness at diastole (IVSd), left ventricular end-systolic internal diameters (LVIDs), left ventricular end-diastolic internal diameters (LVIDd), left ventricular posterior wall end-diastolic thickness (LVPWd), left ventricular ejection fraction (LVEF), and left ventricular cardiac output (LVCO). All parameters were measured for 3 consecutive cardiac cycles unaffected by respiration, and the mean values were calculated. Four weeks after the intervention, echocardiography was repeated. After completing the experiment, the experimental rats were euthanized using carbon dioxide suffocation method to minimize suffering.

Strain analysis assessed by echocardiographic speckle tracking

Strain analysis was performed with VINNO M86E (Vinno, Suzhou, China) by tracing left ventricular wall motion over three consecutive cardiac cycles. The endocardial and epicardial boundaries were traced manually. The software automatically analyzed the strain in the longitudinal and circumferential direction of each segment [13]. The average strain value of the left ventricular myocardium was calculated from the mean of the three cardiac cycles.

The evaluation of oxygen saturation via photoacoustic imaging

PA images were obtained using excitation wavelengths at 750- and 850-nm, which correspond to the maximal absorption of oxyhemoglobin and deoxyhemoglobin, respectively. The imaging was performed using an array transducer with a central frequency of 20 MHz (MX250) in oxy-hemo mode to determine oxygen saturation (sO_2) [14]. The gain for the PA signal acquisition was set to 40 dB, with a 2D gain of 22 dB. A B-mode was also performed for colocalization of photoacoustic signals.

Morphologic alterations detected by H&E staining and electron microscopy

For light microscopic investigations, border tissues of infarct samples were initially fixed in 10% formaldehyde. Subsequently, these tissues were dehydrated using ascending concentrations of alcohol, followed by clarification in toluene and finally, embedded in paraffin. 5 μm paraffin-embedded tissue sections were prepared, followed by dewaxing, rehydration, and hematoxylin and eosin (H&E) staining. Subsequently, the stained sections were examined with an Olympus BH-2 microscope (Tokyo, Japan). All sections were evaluated by an experienced histologist, who was blinded to the sample identities, to characterize the histopathologic alterations.

LV border tissues of the infarcted area were fixed in a 2.5% glutaraldehyde solution at 4°C overnight and then postfixed in cacodylate buffer with 1% osmium tetroxide for 1 h for subsequent assay. Then samples were dehydrated through a graded ethanol series, embedded in Epon medium and dissected into 60-70 nm sections. These sections were stained with uranyl acetate and lead citrate. Tissues were imaged using an electron microscope (JEM-1200EX; JEOL Company, Japan). Ultra-structural changes of the diaphragm tissue were observed and documented. Mitochondrial da-

Table 1. Left ventricular structural parameters assessed by echocardiography and biochemical indices

	IVSd (mm)	LVDd (mm)	LVDs (mm)	LVPWd (mm)	cTn-T (ng/ml)	NT-proBNP (pg/ml)
Control	1.88±0.11	4.36±0.75	2.35±0.61	2.02±0.26	1.43±0.29	59.23±17.03
Model	1.33±0.20*	7.11±1.43*	5.68±1.43*	2.19±0.33	3.92±1.15*	615.37±213.24*

Data are expressed as mean ± SD. n = 10 in the control group and 12 in the model group. *P<0.05 vs. control group. IVSd, interventricular septal thickness at diastole; LVDd, left ventricular end-diastolic diameter; LVDs, left ventricular end-systolic diameter; LVPWd, left ventricular posterior wall thickness at diastole; cTn-T, cardiac troponin T; NT-pro BNP, N-terminal pro-B-type natriuretic peptide.

mage was quantified using the Flameng scoring system to assess the severity of injury [15]. Each sample was observed for five distinct fields of view, with twenty mitochondria chosen from each for numerical assessment. The scoring criteria were as follows: Grade 0 (0 points) indicated preserved mitochondrial structure and particle integrity. Grade I (1 point) indicated intact structures with particle loss, alongside mild swelling, diminished density of the matrix, and slight separation of cristae. Grade II (2 points) was marked by a moderate mitochondrial swelling with translucent matrices. Grade III (3 points) involved disruptions within the mitochondrial cristae and densification of the matrix. Grade IV (4 points) denoted significant mitochondrial damage with extensive cristae destruction and breaches in both internal and external membranes.

Infarct size and fibrosis detected by Masson's trichrome staining

Collagen deposition in the border zone of infarcted myocardium was analyzed. 5 μm LV sections were stained using Masson's trichrome staining kit. The infarct size and collagen deposition were quantified using Image J.

Quantification of cardiac troponin T and N-terminal pro-B-type natriuretic peptide in serum

The concentrations of cardiac troponin T (cTn-T) and N-terminal pro-B-type natriuretic peptide (NT-proBNP) in serum were determined using commercial enzyme-linked immunosorbent assay (ELISA) kits. All assays were executed in accordance with the manufacturer's protocols. Serial dilutions of standards were included to ensure the accuracy and reliability of the assay. The levels in the test samples were subsequently calculated with reference to these standard curves.

Statistical analysis

Data were tested for normal distribution using the Shapiro-Wilk test, and expressed as mean ± standard deviation (SD) when adhering to a normal distribution. The variance homogeneity was determined using F test or Welch t test. The two independent samples t-test or Welch t-test was used for comparison of each measurement between two groups. Pearson correlation analysis was used to evaluate the correlations between echocardiographic multimodal parameters, histopathologic assessments, and serum biomarkers in model group. A *p*-value of <0.05 was considered a significant difference. Both experts, proficient in echocardiographic or histopathologic analysis, collaborated to ensure the accuracy and reliability of this study.

Results

Routine echocardiography and serum biomarker analyses revealed significant structural and functional changes in the model group

Throughout the study period, eight rats died in the model group, whereas no rats died in the control group. Ultrasound-derived cardiac dimensions and circulating cardiac biomarker levels are presented in **Table 1**. In the control group, IVSd, LVDd, LVDs, and LVPWd were 1.88±0.11 mm, 4.36±0.75 mm, 2.35±0.61 mm, and 2.02±0.26 mm respectively. In contrast, the model group demonstrated a significant reduction in IVSd to 1.33±0.20 mm and marked increases in both LVDd and LVDs to 7.11±1.43 mm and 5.68±1.43 mm, respectively (all P<0.05). LVPWd experienced a marginal increase, which did not reach statistical significance.

Additionally, the serum concentration of cTn-T and NT-proBNP in the control group was 1.43±0.29 ng/mL and 59.23±17.03 pg/mL,

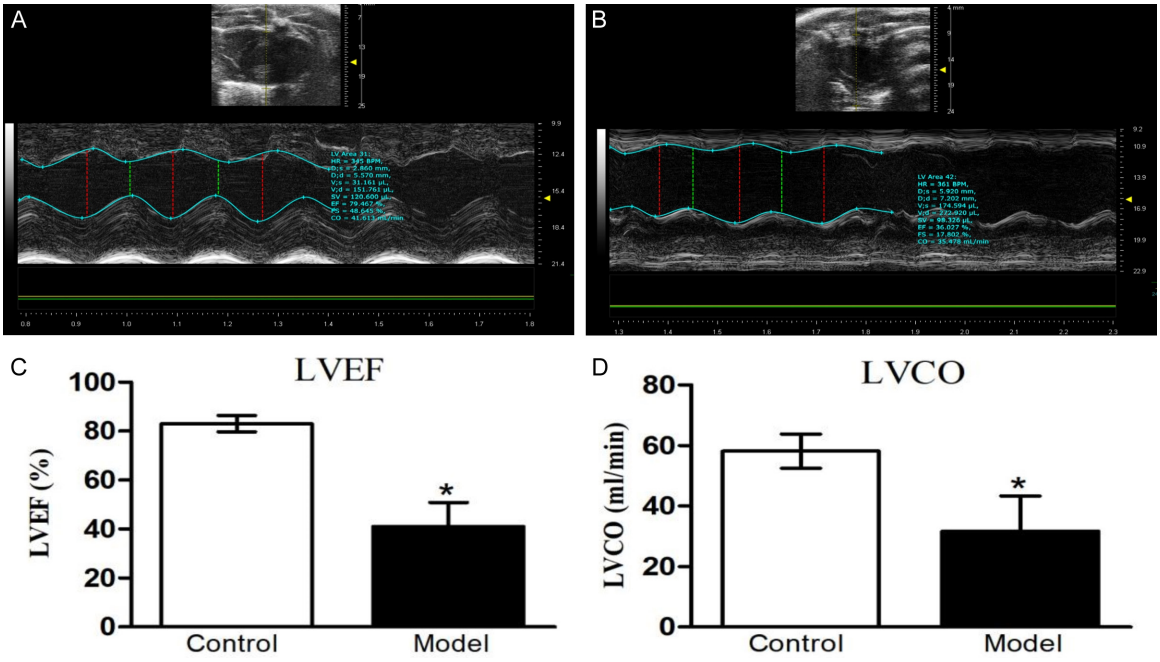

Figure 1. Echocardiographic analysis of left ventricular systolic function. A. Representative M-mode echocardiographic image of a control rat. B. Representative M-mode echocardiographic image of a model rat. C. Left ventricular ejection fraction (LVEF). D. Left ventricular cardiac output (LVCO). Data are presented as mean ± standard deviation. The control group includes 10 rats, while the model group includes 12 rats. *P<0.05 compared to the control group. LVEF: left ventricular ejection fraction; LVCO: left ventricular cardiac output.

respectively. In contrast, the model group demonstrated significantly higher levels of these biomarkers, with cTn-T rising to 3.92±1.15 ng/mL and NT-proBNP to 615.37±213.24 pg/mL (all P<0.05), indicative of cardiac injury and functional impairment.

The alterations in left ventricular function, as determined by echocardiography, are illustrated in **Figure 1**. In comparison to the control group, the model group showed significant decreases in LVEF and LVCO by 50.56% and 54.44%, respectively.

Speckle tracking echocardiography revealed reduced myocardial strain, while PA imaging indicated diminished myocardial oxygen saturation

Myocardial strain was assessed using echocardiographic speckle tracking (**Figure 2A-F**). The comparative analysis of GLS and GCS between the two groups uncovered marked discrepancies. The strain patterns in the model group were notably scattered, discrete, and lacked synchronicity compared to the control group. GLS in the model cohort was significantly diminished compared to the control group (-13.08%±2.39% vs. -18.54%±1.48%, P<0.05). Furthermore, the model group demonstrated a significantly reduced GCS when compared to the control group (-17.26%±1.57% vs. -22.63%±1.17%, P<0.05).

sO_2 levels in rats were evaluated using an integrated photoacoustic imaging/ultrasound (PAI/US) system (**Figure 2G-I**). In the control group, the anterior wall exhibited an sO_2 of 68.13%±3.11%. In contrast, sO_2 in the anterior wall of model rats decreased significantly, which was recorded at 58.48%±5.99%. For the model group, the sO_2 readings of the posterior wall were slightly reduced when compared to the control group, yet this difference was not statistically significant.

Histopathologic analyses revealed necrosis of cardiomyocytes and mitochondrial damage

Under light microscope, the myocardial tissue of the control group was intact, the transverse stripe was clear, neatly arranged, of uniform size, and the nuclei of the cells were centered, with no obvious abnormality observed (**Figure**

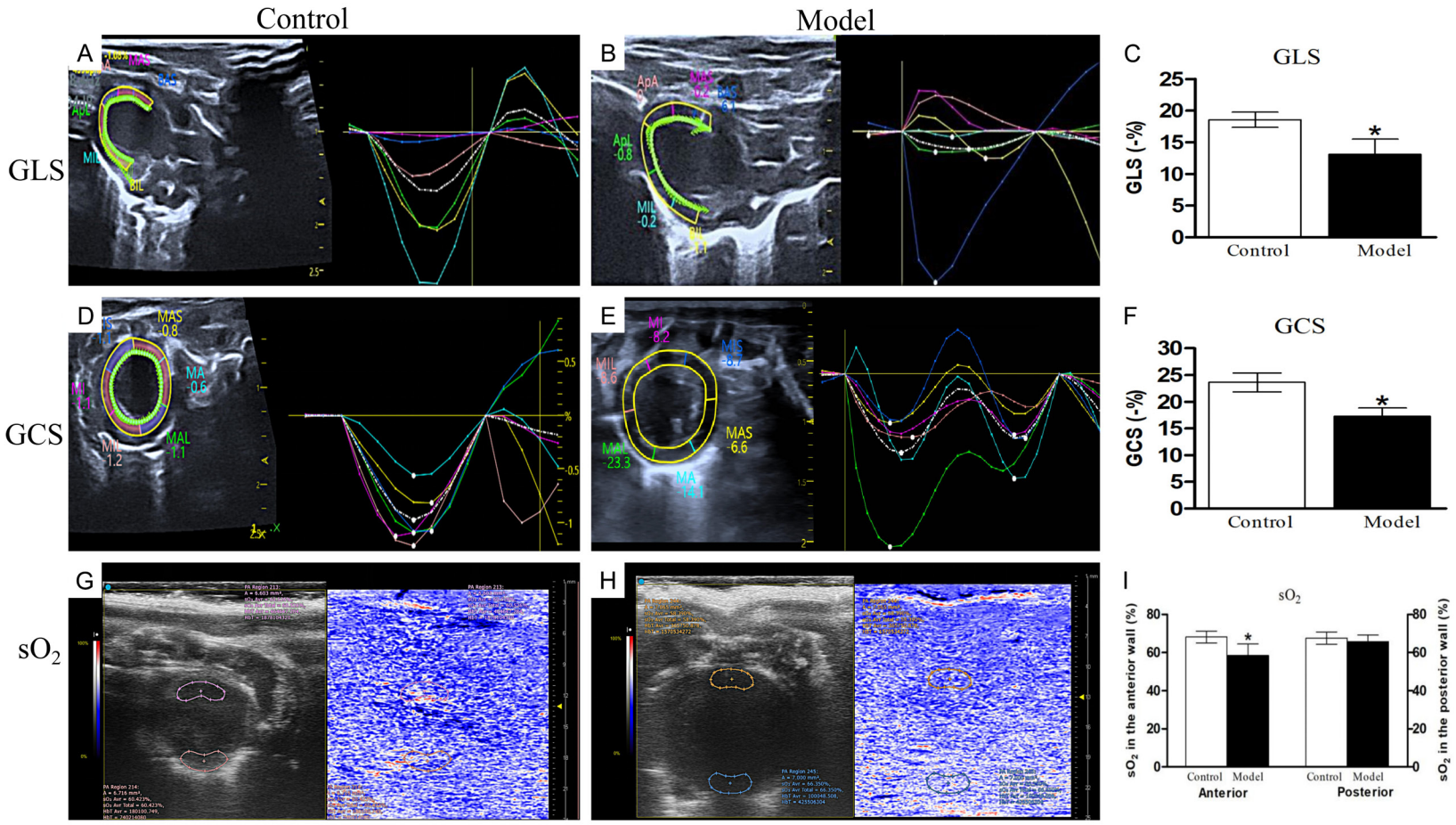

Figure 2. Myocardial strain analysis using speckle tracking and oxygen saturation evaluation by photoacoustic imaging. A. Characteristic speckle tracking strain image of the left ventricular long-axis view in a control rat. B. Characteristic speckle tracking strain image of the left ventricular long-axis view in a model rat. C. Global longitudinal strain (GLS) comparison between the control and model groups. D. Representative speckle tracking strain echocardiography of the left ventricular short-axis view in a control rat. E. Representative speckle tracking strain echocardiography of the left ventricular short-axis view in the model group. F. GCS comparison between the control and model groups. G. Photoacoustic imaging of a control rat, showing a color scale that highlights regions of high (red) and low (blue) myocardial oxygen saturation. H. Photoacoustic imaging of a model rat. I. Oxygen saturation (sO_2) comparison between the control and model groups. Data are presented as mean ± standard deviation. The control group consisted of 10 rats, and the model group consisted of 12 rats. *P<0.05 compared to the control group.

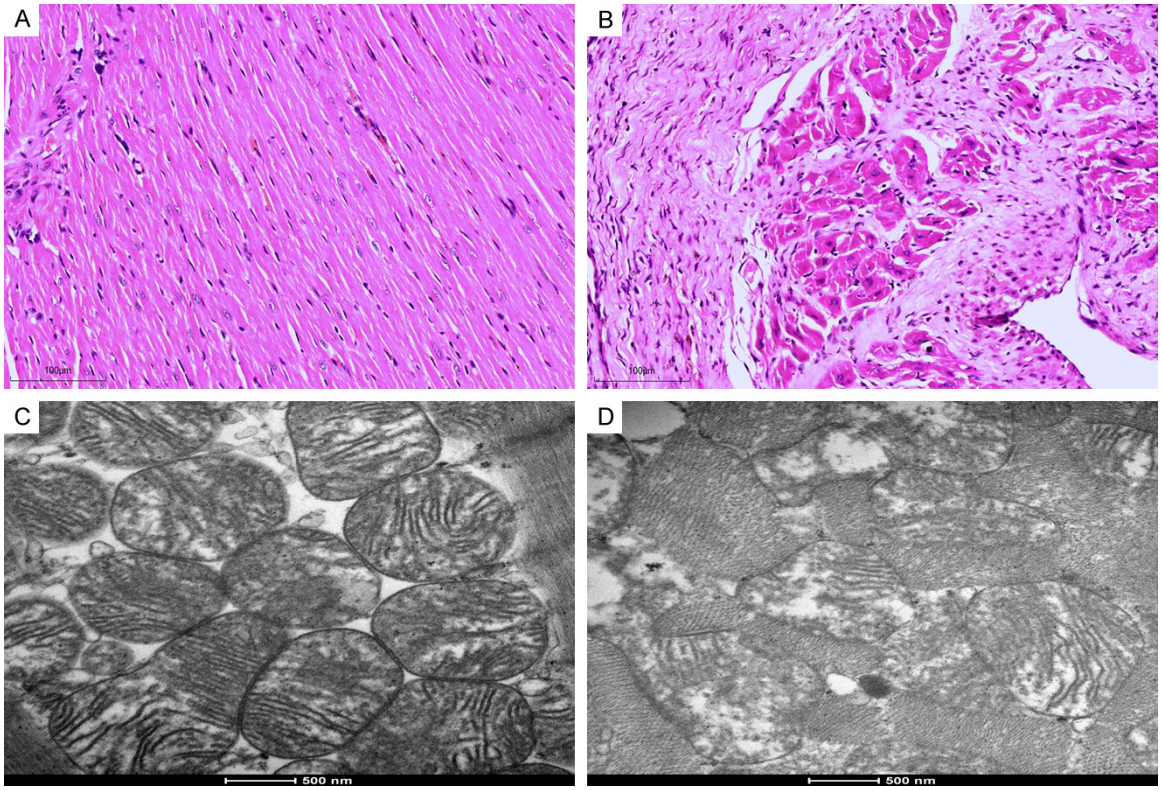

Figure 3. Histologic alterations in the left ventricular myocardium assessed by hematoxylin and eosin (H&E) staining, and mitochondrial damage evaluated using electron microscopy. A. H&E staining of the left ventricular myocardium in the control group. B. H&E staining of the left ventricular myocardium in the model group. C. Mitochondrial integrity assessed by electron microscopy in the control group. D. Mitochondrial integrity assessed by electron microscopy in the model group. Scale bars: H&E stain = 100 μm (×100), electron microscopy = 500 nm (×20,000).

3A). In the model group, myocardial fibers across all layers of the rat myocardium were loosely arranged and disorganized, with blurred transverse striations, obvious swelling, and necrosis of myocardial cells (**Figure 3B**). Additionally, there were interstitial congestion and edema, local myocardial inflammatory cell infiltration, interstitial fibrosis, and the most severe damage was observed in subendocardial myocardium.

Electron microscopy of the sham-operated rats demonstrated well-organized myocardial fibers with prominent sarcomeres and abundant mitochondria. The mitochondria presented a classic elongated structure, featuring continuous cristae along with well-preserved membranes and granules, as illustrated in **Figure 3C**. In model group, a disarray of the myofibrillar architecture with irregular myofilaments and disrupted Z-lines was observed (**Figure 3D**). Mitochondrial abnormalities were prominent, including vacuolation, swelling, and, in some cases, the absence of cristae. The Flameng score was significantly lower in the control group (0.70±0.67) compared to the model group (2.83±1.34), suggesting more extensive mitochondrial damage in the model group.

Masson's trichrome staining revealed increased myocardial fibrosis in the model group

Morphologic analysis of heart tissue in the model group revealed significant changes, including reduced left ventricular wall thickness and extensive fibrous scarring (**Figure 4**). In the model group, the estimated infarct size accounted for 40.07±7.41% of the myocardium. Importantly, cardiac fibrosis increased substantially in the model group, where the collagen volume fraction (CVF) reached 12.56±1.94%, markedly higher than the 2.59±0.29% recorded in the control group ($P<0.05$). These results from Masson's trichrome staining corroborated those obtained from H&E staining, further confirming the successful establishment of the IHF model.

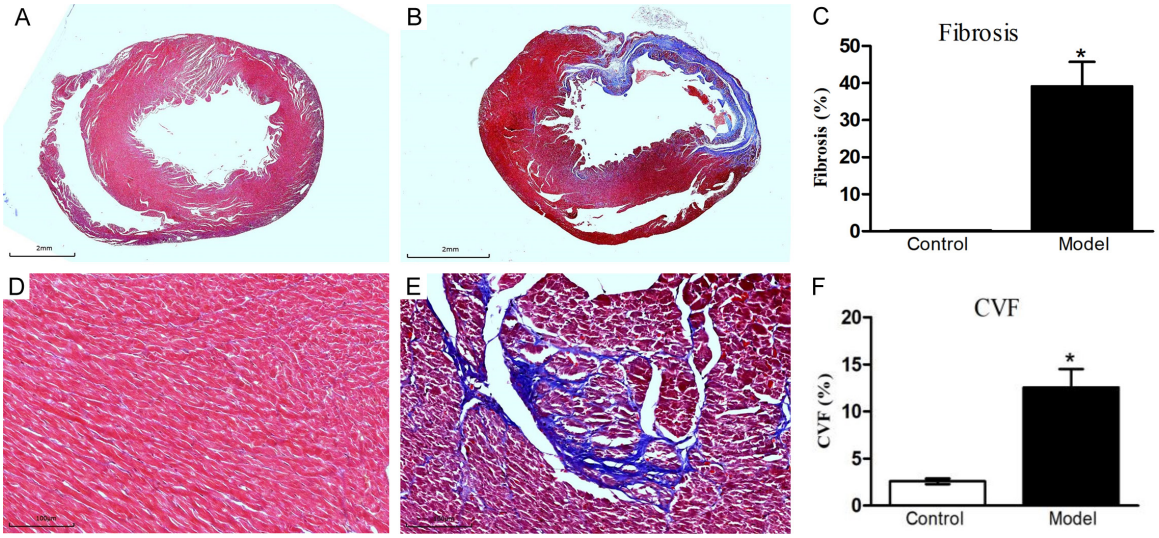

Figure 4. Myocardial fibrosis in the left ventricular myocardium depicted by Masson's trichrome staining. A, D. Myocardial fibrosis identified in the control group. B, E. Myocardial fibrosis identified in the model group. C. Quantification of fibrosis area in the left ventricular myocardium between the two groups. F. Collagen volume fraction (CVF) in the left ventricular myocardium compared between the two groups. Data are presented as mean ± standard deviation, with n = 10 in the control group and n = 12 in the model group. *P<0.05 compared to the control group.

Correlation analysis revealed significant associations between echocardiographic parameters, histopathologic alterations, and serum biomarkers in the model group

Figure 5 shows the correlations between echocardiographic multimodal parameters, histopathological assessments, and serum biomarkers in the model group. LVCO demonstrated significant negative associations with mitochondrial damage grades, CVF, and pro BNP ($r = -0.73$, $P<0.01$; $r = -0.58$, $P<0.05$; $r = -0.59$, $P<0.05$, respectively).

GLS demonstrated the strongest correlations with myocardial injury indicators. It exhibited negative correlations not only with mitochondrial injury grading and CVF ($r = -0.72$, $P<0.01$; $r = -0.64$, $P<0.05$) but also with CTNT and pro BNP ($r = -0.6$, $P<0.05$; $r = -0.81$, $P<0.01$). GCS showed negative relationships with cTNT and pro BNP ($r = -0.70$, $P<0.05$; $r = -0.73$, $P<0.01$). However, anterior wall SO_2 did not exhibit notable correlations with histopathologic damage or serum biomarkers.

Discussion

According to the World Health Organization's 2020 rankings, ischemic heart disease was identified as the leading cause of death worldwide, accounting for 16% of all mortalities [16]. Hence, comprehensive research into the etiology, pathophysiology, treatment, outcome, and prevention of ischemic heart disease holds significant importance. The establishment of animal models, particularly rat models of IHF, plays a crucial role in cardiac disease research. After seeking medical attention in the early stages of acute myocardial infarction, doctors can promptly provide symptomatic treatment, such as pain relief and vasodilation, to alleviate the patient's pain. Delaying medical care, however, can result in greater suffering. This study found that ligation of the left anterior descending coronary artery in rats induced a reduction in LVEF and cardiac output after four weeks, accompanied by myocardial cell necrosis, mitochondrial damage, and interstitial fibrosis. Furthermore, we employed speckle tracking echocardiography and photoacoustic imaging techniques to investigate changes in global myocardial strain and blood oxygen saturation in the ischemic heart disease IHF model rats. Our results demonstrated a reduction in GLS and GCS in IHF rats, with decreased oxygenation in ischemic regions. Relationships were also noted between LVCO, GLS, GCS, and pathologic features such as interstitial fibrosis and mitochondrial injury, with GLS showing the most pronounced correlation with pathology. However, sO_2 levels in anterior wall showed no significant correlation with pathological chang-

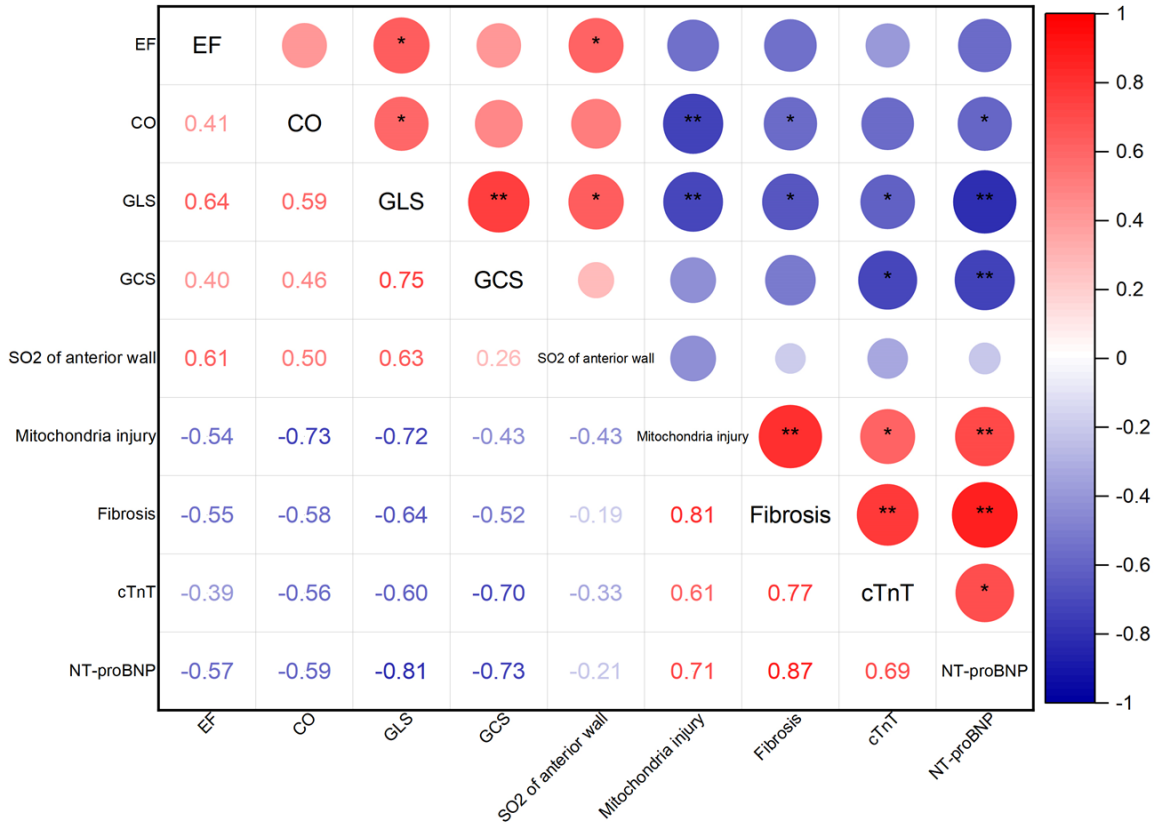

Figure 5. Correlations between ultrasonic multimodal parameters, pathologic features, and serum biomarkers. Pearson's correlation tests were employed to statistically assess the relationships between echocardiographic parameters, pathologic characteristics, and serum biomarkers. The correlation coefficients (lower left) and significance levels (upper right) for each paired comparison, with $^{*}P$ indicating <0.05, and $^{**}P$<0.01.

es. The novelty of this study lies in the comprehensive assessment of cardiac function using multiple echocardiographic indices and their correlation with pathologic changes. By integrating conventional echocardiography, strain imaging, and photoacoustic imaging techniques, we were able to more comprehensively monitor left ventricular function and accurately reflect pathologic alterations, thereby providing precise monitoring of disease progression and treatment efficacy.

LVCO was negatively related to mitochondrial damage grade and CVF

Routine echocardiography, which evaluates LVEF and LVCO, is the primary imaging technique for assessing left ventricular systolic function and plays a pivotal role in the diagnosing heart failure. However, LVEF and LVCO are indirect indicators, inferred from changes in the LV cavity internal diameter. They are significantly influenced by left ventricular volume and heart rate variations, and do not offer a precise, comprehensive analysis of left ventricular function [17]. Moreover, LVEF can appear normal or even elevated in the initial stages of certain cardiovascular diseases due to myocardial compensation [18]. The current study found that LVEF and LVCO were markedly reduced in the model group compared to control rats, albeit with high standard deviations within the model group, indicating substantial intra-group variability. This result agrees with the variability observed in previous research and suggests a potential correlation with the diverse degrees of ischemia stemming from varying coronary anatomy of rats [19]. Notably, our study revealed that in contrast to LVEF, there was a more substantial correlation between LVCO and the severity of mitochondrial damage, CVF, and pro-BNP levels. This finding aligns with

prior studies highlighting the detrimental impact of mitochondrial dysfunction and fibrosis on cardiac performance [20]. The reason may be that LVCO reflects the actual volume of blood pumped by the heart per unit time, providing a direct quantification of cardiac efficiency, while LVEF merely calculates the proportion of blood pumped out during systole [21].

Myocardial strain exhibits a strong correlation with pathologic alterations

Speckle tracking strain analysis assesses myocardial motion in radial, circumferential, and longitudinal directions, presenting a novel, high-throughput, and sensitive method for detecting myocardial dynamics [22]. Impaired myocardial contractility, increased stiffness, and structural changes of the myocardium result in diminished myocardial deformation. Our study illustrated that both GLS and GCS were reduced in IHF model rats, indicating impaired myocardial deformation longitudinally and circumferentially. Notably, GLS presented a stronger negative correlation with pathologic changes, such as mitochondrial damage and fibrosis, as well as cardiac biomarkers like cTn-T and proBNP, compared to cardiac output. This implies that GLS may detect subtle myocardial functional and mechanical alterations with higher sensitivity. Our findings highlight the ability of myocardial strain analysis to provide a superior assessment of pathologic remodeling in heart failure, outperforming traditional metrics like cardiac output.

This study, similar to the research conducted by Bauer et al., suggests that strain analysis is more sensitive than traditional echocardiographic methods in detecting overall changes in myocardial function and pathologic alteration [23]. It enables precise regional analysis of both infarcted and unaffected myocardial areas [24]. Furthermore, myocardial strain facilitates earlier identification of the treatment effectiveness [25]. Longitudinal strain is primarily associated with deformation of myocardial fibers in the endocardium; circumferential strain is mainly related to deformation of myocardial fibers in the mid-layer and the epicardium; and radial strain reflects the overall coordinated movement of myocardial fibers throughout all layers [26]. Thus, strain changes in the three dimensions are valuable in assessing which myocardial layer is affected. Our study demonstrates that LAD ligation impairs all three myocardial layers, as confirmed by Masson's trichrome staining, leading to reduced longitudinal and circumferential strain. In contrast, radial strain was excluded from analysis due to significant inter-observer and intra-observer variability and limited reproducibility. In addition, GLS in the model group decreased by 26.95% while GCS by 23.73%, as compared to the control group. GLS showed a greater reduction than GCS, suggesting higher vulnerability or sensitivity of endocardium than the mid-layer and the epicardium to the modeled pathology [27].

sO_2 in the anterior wall showed no significant correlation with LV histopathologic damage

Photoacoustic imaging (PAI) is an emerging noninvasive modality that exploits near-infrared light for elucidating the functional status of tissues through detection of oxygenated and deoxygenated hemoglobin. It synergistically leverages the superior contrast of optical imaging and the deep tissue penetration of ultrasound. This duality allows for real-time structural and functional insights, particularly advantageous for exploring myocardial ischemia and hypoxia.

Significant for its clinical relevance, Al Mukaddim et al. demonstrated the sensitivity of PAI in detecting acute myocardial ischemic events [28], while David et al. extended its application to the evaluation of hypoxia across multiple organs including brain, kidneys, and liver post-infarction [29]. In concordance with the existing literature, our study reveals a pronounced drop in sO_2 of the anterior wall myocardium of model rats.

Surprisingly, there are no significant correlations between sO_2 and histopathologic damage or serum biomarkers, which contradicts the anticipated negative correlation. This discrepancy may be due to the timing of sO_2 measurements relative to the onset of myocardial ischemia. It has reported that sO_2 in the anterior wall decreased from 74.7% before MI to 19.9% one day after MI, and begins to recover 7 days after MI as adaptive responses such as neoangiogenesis occur [30]. Our findings thus highlight the multifarious nature of myocardial oxygenation in the context of cardiac pathology, and underscore the need to interpret PAI data

within the broader context of physiologic and temporal factors.

Conclusions

Our study revealed abnormalities in left ventricular myocardial strain and local tissue oxygen saturation (sO_2) in an IHF model induced by left anterior descending branch ligation. GLS originates from myocardial strain analysis and is a sensitive indicator of pathologic myocardial remodeling in heart failure. However, an unexpected finding of our study was the lack of significant correlation between local myocardial sO_2 and potential pathologic changes, suggesting limitations in the current application of sO_2 as a diagnostic marker.

The limitation of our research was the lack of cross-validation using advanced imaging techniques, such as labeled magnetic resonance imaging (t-MRI) and cardiac magnetic resonance tissue tracking (CMR-TT). It is worth noting that good consistency has been demonstrated between the myocardial strain parameters obtained through CMR-TT, STE, and t-MRI measurements. In addition, our study did not fully explore the potential of multimodal ultrasound analysis, including technologies such as contrast-enhanced ultrasound, three-dimensional imaging, coronary artery blood flow reserve measurement, and artificial intelligence analysis. These technologies represent the future direction of our research.

Overall, our findings confirm that left ventricular strain is associated with cardiac function and pathologic remodeling. It is expected that myocardial staining analysis may ultimately supplement or even replace LVEF as a diagnostic indicator for heart failure, positioning it as an important tool for evaluating IHF.

Acknowledgements

This work was funded by the National Natural Science Foundation of China (82174469).

Disclosure of conflict of interest

The authors declare that the research was conducted in the absence of any commercial or financial relationships that could be construed as a potential conflict of interest.

Address correspondence to: Luting Zhang, Ultrasound Department, The Second Affiliated Hospital of Fujian University of Traditional Chinese Medicine, Fuzhou 350003, Fujian, China. Tel: +86-0591-8787-8130; E-mail: zhangluting39@gmail.com; Hongjia Zhao, Fujian University of Traditional Chinese Medicine, Fuzhou 350122, Fujian, China. Tel: +86-13788886031; E-mail: hongjiafz@163.com

References

[1] Groenewegen A, Rutten FH, Mosterd A and Hoes AW. Epidemiology of heart failure. Eur J Heart Fail 2020; 22: 1342-1356.
[2] Jenca D, Melenovsky V, Stehlik J, Stanek V, Kettner J, Kautzner J, Adamkova V and Wohlfahrt P. Heart failure after myocardial infarction: incidence and predictors. ESC Heart Fail 2021; 8: 222-237.
[3] Muthuramu I, Lox M, Jacobs F and De Geest B. Permanent ligation of the left anterior descending coronary artery in mice: a model of post-myocardial infarction remodelling and heart failure. J Vis Exp 2014; 52206.
[4] Lowe JE, Reimer KA and Jennings RB. Experimental infarct size as a function of the amount of myocardium at risk. Am J Pathol 1978; 90: 363-379.
[5] Peng C, Cai Q, Chen M and Jiang X. Recent advances in tracking devices for biomedical ultrasound imaging applications. Micromachines (Basel) 2022; 13: 1855.
[6] Leader CJ, Moharram M, Coffey S, Sammut IA, Wilkins GW and Walker RJ. Myocardial global longitudinal strain: an early indicator of cardiac interstitial fibrosis modified by spironolactone, in a unique hypertensive rat model. PLoS One 2019; 14: e0220837.
[7] Fu L, Ruan Q, You Z, Huang H, Chen Y, Cheng S, Yan L, Cai H, Chen Y, Lin D, Chen H and Huang C. Investigation of left ventricular strain and its morphological basis during different stages of diastolic and systolic dysfunction in spontaneously hypertensive rat. Am J Hypertens 2022; 35: 423-432.
[8] Lin L and Wang LV. The emerging role of photoacoustic imaging in clinical oncology. Nat Rev Clin Oncol 2022; 19: 365-384.
[9] Wu M, Awasthi N, Rad NM, Pluim JPW and Lopata RGP. Advanced ultrasound and photoacoustic imaging in cardiology. Sensors (Basel) 2021; 21: 7947.
[10] Rix A, Lederle W, Theek B, Lammers T, Moonen C, Schmitz G and Kiessling F. Advanced ultrasound technologies for diagnosis and therapy. J Nucl Med 2018; 59: 740-746.
[11] Khan MS, Smego D, Ishidoya Y, Hirahara AM, Offei E, Ruiz Castillo MS, Gharbia O, Li H, Palatinus JA, Krueger L, Hong T, Hoareau GL, Ranjan R, Selzman CH, Shaw RM and Dosdall DJ. A canine model of chronic ischemic heart failure. Am J Physiol Heart Circ Physiol 2023; 324: H751-H761.

[12] Hegemann N, Bintig W, Perret PL, Rees J, Viperino A, Eickholt B, Kuebler WM, Hopfner M, Nitzsche B and Grune J. In-ovo echocardiography for application in cardiovascular research. Basic Res Cardiol 2023; 118: 19.
[13] Ahmad SM, Farag EM, Eltahlawi MA and Salama AE. Assessment of left ventricular function by global longitudinal strain in patients with non-ST elevation myocardial infarction. Egyptian Journal of Hospital Medicine 2022; 86: 222-227.
[14] Lv J, Peng Y, Li S, Guo Z, Zhao Q, Zhang X and Nie L. Hemispherical photoacoustic imaging of myocardial infarction: in vivo detection and monitoring. Eur Radiol 2018; 28: 2176-2183.
[15] Zheng L, Li B, Lin S, Chen L and Li H. Role and mechanism of cardiac insulin resistance in occurrence of heart failure caused by myocardial hypertrophy. Aging (Albany NY) 2019; 11: 6584-6590.
[16] Rana JS, Khan SS, Lloyd-Jones DM and Sidney S. Changes in mortality in top 10 causes of death from 2011 to 2018. J Gen Intern Med 2021; 36: 2517-2518.
[17] Cikes M and Solomon SD. Beyond ejection fraction: an integrative approach for assessment of cardiac structure and function in heart failure. Eur Heart J 2016; 37: 1642-1650.
[18] Marwick TH. Ejection fraction pros and cons: JACC state-of-the-art review. J Am Coll Cardiol 2018; 72: 2360-2379.
[19] Kainuma S, Miyagawa S, Fukushima S, Tsuchimochi H, Sonobe T, Fujii Y, Pearson JT, Saito A, Harada A, Toda K, Shirai M and Sawa Y. Influence of coronary architecture on the variability in myocardial infarction induced by coronary ligation in rats. PLoS One 2017; 12: e0183323.
[20] Osterholt M, Nguyen TD, Schwarzer M and Doenst T. Alterations in mitochondrial function in cardiac hypertrophy and heart failure. Heart Fail Rev 2013; 18: 645-656.
[21] Mele D, Nardozza M and Ferrari R. Left ventricular ejection fraction and heart failure: an indissoluble marriage? Eur J Heart Fail 2018; 20: 427-430.
[22] Thavendiranathan P, Poulin F, Lim KD, Plana JC, Woo A and Marwick TH. Use of myocardial strain imaging by echocardiography for the early detection of cardiotoxicity in patients during and after cancer chemotherapy: a systematic review. J Am Coll Cardiol 2014; 63: 2751-2768.
[23] Bauer M, Cheng S, Jain M, Ngoy S, Theodoropoulos C, Trujillo A, Lin FC and Liao R. Echocardiographic speckle-tracking based strain imaging for rapid cardiovascular phenotyping in mice. Circ Res 2011; 108: 908-916.
[24] Diao KY, Yang ZG, Ma M, He Y, Zhao Q, Liu X, Gao Y, Xie LJ and Guo YK. The diagnostic value of global longitudinal strain (GLS) on myocardial infarction size by echocardiography: a systematic review and meta-analysis. Sci Rep 2017; 7: 10082.
[25] Nesbitt GC, Mankad S and Oh JK. Strain imaging in echocardiography: methods and clinical applications. Int J Cardiovasc Imaging 2009; 25 Suppl 1: 9-22.
[26] Zhang K, Sheu R, Zimmerman NM, Alfirevic A, Sale S, Gillinov AM and Duncan AE. A comparison of global longitudinal, circumferential, and radial strain to predict outcomes after cardiac surgery. J Cardiothorac Vasc Anesth 2019; 33: 1315-1322.
[27] Gherbesi E, Gianstefani S, Angeli F, Ryabenko K, Bergamaschi L, Armillotta M, Guerra E, Tuttolomondo D, Gaibazzi N, Squeri A, Spaziani C, Pizzi C and Carugo S. Myocardial strain of the left ventricle by speckle tracking echocardiography: from physics to clinical practice. Echocardiography 2024; 41: e15753.
[28] Mukaddim RA, Rodgers A, Hacker TA, Heinmiller A and Varghese T. Real-time in vivo photoacoustic imaging in the assessment of myocardial dynamics in murine model of myocardial ischemia. Ultrasound Med Biol 2018; 44: 2155-2164.
[29] David H, Ughetto A, Gaudard P, Plawecki M, Paiyabhroma N, Zub E, Colson P, Richard S, Marchi N and Sicard P. Experimental myocardial infarction elicits time-dependent patterns of vascular hypoxia in peripheral organs and in the brain. Front Cardiovasc Med 2020; 7: 615507.
[30] Hackfort BT, Chalise U, Daseke MJ and Lindsey ML. Myocardial oxygen saturation measured by photoacoustic EKV imaging. FASEB J 2020; 34: 1.